Donor/Acceptor Effects on the Linear and Nonlinear Optical Properties of Geminal Diethynylethenes (g-DEEs)

by **Yuming Zhao***[a]), **Ningzhang Zhou**[a]), **Aaron D. Slepkov**[b]), **Sorin C. Ciulei**[c]), **Robert McDonald**[d]), **Frank A. Hegmann***[b]), and **Rik R. Tykwinski***[c])

[a]) Department of Chemistry, Memorial University of Newfoundland, St. John's, NL A1B 3X7, Canada (e-mail: yuming@mun.ca)

[b]) Department of Physics, University of Alberta, Edmonton, AB T6G 2J1, Canada (fax: (+1) 780-492-0714; e-mail: hegmann@phys.ualberta.ca)

[c]) Department of Chemistry, University of Alberta, Edmonton, AB T6G 2G2, Canada (fax: (+1) 780-492-8231; e-mail: rik.tykwinski@ualberta.ca)

[d]) X-Ray Crystallography Laboratory, Department of Chemistry, University of Alberta, Edmonton, AB T6G 2G2, Canada

A series of geminal diethynylethenes (g-DEEs) with electron-donating and/or electron-accepting (D/A) groups were synthesized *via* a Pd-catalyzed cross-coupling sequence. The UV/VIS spectra for donor–acceptor (D–A) functionalized g-DEEs **5**, **8**, and **11** show distinctive absorption trends attributable to intramolecular charge-transfer (ICT). The bond-length-alternation (BLA) index for the cross-conjugated enediyne framework varies slightly with different terminal substituents as determined by density-functional theory (DFT) calculations and single-crystal X-ray analysis. Ultrafast third-order optical nonlinearities for the g-DEEs were measured by the differential optical *Kerr* effect (DOKE) technique and show that terminal donor–acceptor substitution of g-DEEs enhances molecular second hyperpolarizabilities (γ) in comparison to donor or acceptor g-DEEs. A small increase in the two-photon-absorption cross-section ($\sigma^{(2)}$) is observed in the series **9**–**11** as a result of increased functionalization. The effects of donor/acceptor substitution on electron delocalization along the cross-conjugated enediyne structure are evaluated on the basis of natural-bond-orbital (NBO) analysis. Solid-state structures of the four derivatives **3b**, **4b**, **7** and **8** were characterized by single-crystal X-ray structural analysis and show an asymmetric unit cell for one derivative, D–A g-DEE **8**.

1. Introduction. – Conjugated molecules with highly delocalized and polarizable π-electron systems are prospects for third-order nonlinear optical (NLO) materials, and could form the basis for achieving ultrafast all-optical-based computing and telecommunications technology [1][2]. To find ideal and applicable organic NLO materials, a large number of organic chromophores have been extensively explored, with many efforts focused on linearly conjugated aromatic and/or nonaromatic π-conjugated systems [2–5]. In assessing the suitability of an organic material for NLO purposes, its efficiency/transparency trade-off at a specific wavelength is an important factor to be considered, and maintaining transparency in the visible region of the spectrum is a significant challenge [6]. Many linearly π-conjugated chromophores tend to perform poorly in this respect, and the pursuit of alternative molecular designs has become more and more appealing and important. In particular, the use of cross-

conjugated π-systems, the topological isomers of linearly conjugated molecules, has been explored [7–10]. One promising aspect of using cross-conjugation in place of linear conjugation lies in the satisfactory electronic transparency arising from the moderated conjugative π-pathway.

We have reported the synthesis and optical properties of cross-conjugated iso-poly(diacetylene) oligomers (iso-PDAs) with pendent methyl and phenyl substituents (see **1** and **2**) [10][11]. The more stable and soluble series **2** displays a superlinear, albeit modest increase in second hyperpolarizability (γ) as a function of chain length (up to $n = 15$), while electronic transparency (absorptivity in the visible region of the spectrum) is maintained at a satisfactory level [10]. With the structure–property relationships as a function of chain length established, the task of revealing the impact of π-electron-donating (D) and -accepting groups (A) appended to cross-conjugated enynes has now been targeted [12]. Such 'push-pull' functionalization is a well-established mode for dictating the electronic characteristics and molecular hyperpolarizabilities for various linearly conjugated molecules [5]. Our work [13], and that of others [7][14][15], has suggested that D/A-substitution can cause notable changes in the electronic-absorption behavior of cross-conjugated oligomers as well.

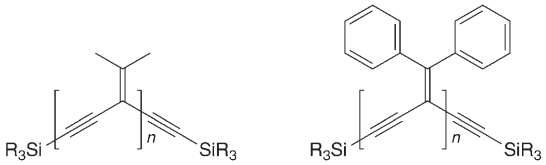

1 **2**

iso-poly(diacetylene) (iso-PDA)

In this paper, we report on a series of electron-donor 4-(dimethylamino)phenyl and ferrocenyl- and/or electron-acceptor (4-nitrophenyl)-substituted geminal diethynylethenes (g-DEEs; see **3**–**11**) that have been synthesized *via* a sequence of Pd-catalyzed cross-coupling reactions. The electronic-absorption properties of these D/A- and D–A-substituted g-DEEs are characterized by UV/VIS spectroscopy, and the structural properties of several derivatives in the solid state are studied by X-ray crystallography. Second-order molecular hyperpolarizabilities (γ) and two-photon-absorption cross-sections ($\sigma^{(2)}$) are determined by the differential optical *Kerr* effect (DOKE) detection technique. Finally, the electron-delocalization characteristics throughout the geminal enediyne π-bridge have been investigated by means of density-functional theory (DFT) calculations and natural-bond-orbital (NBO) analysis.

Results and Discussion. – 2.1. *Synthesis of D/A Substituted g-DEEs.* D/A-Substituted g-DEE molecules **3**–**11** were prepared by using one of two routes (*Scheme*)[1]). In the first case, vinyl triflate **12a** [16] or **12b** [10] was used as the essential building block, to which the appropriate acceptor or donor group could be attached *via* Pd-catalyzed *Sonogashira* coupling with the respective terminal alkynes, to give **3a**, **4a**, **6**, and **10**. Mono-substituted g-DEEs **6** or **10** were then desilylated and cross-coupled to

[1]) The synthesis of compounds **3b**, **4b**, and **5** has been previously communicated, see [13].

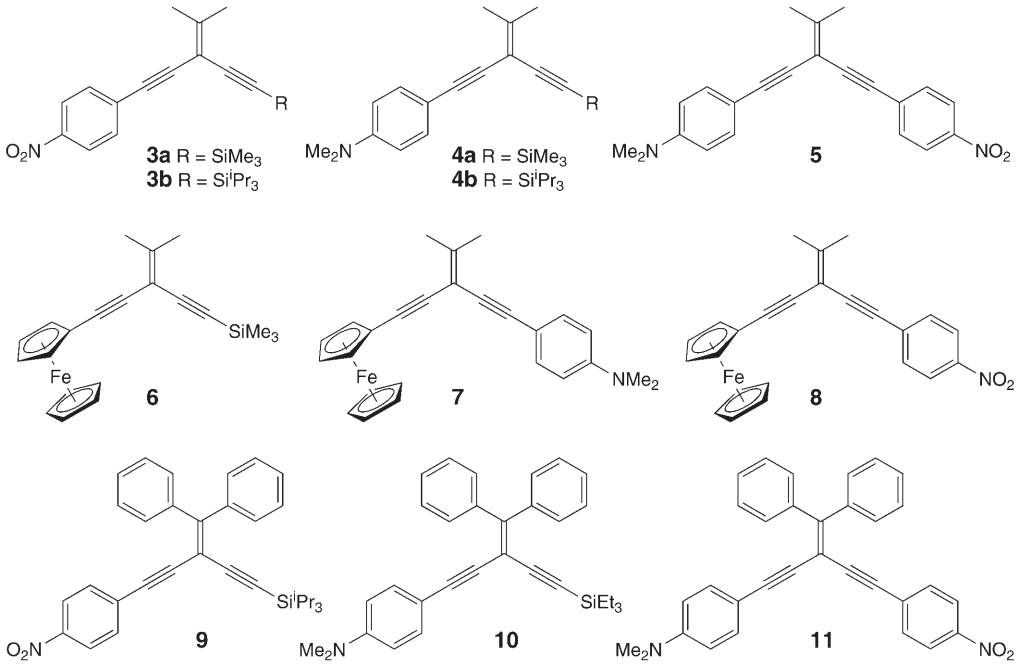

give disubstituted g-DEEs **7**, **8**, and **11**. Alternatively, enediyne **13a** [17] or **13b** [10] could be selectively desilylated and cross-coupled to give g-DEEs **3b**, **4b**, and **9**. Donor substituted **3b** was then carried on to D – A **5** *via* removal of the triisopropylsilyl group with Bu_4NF and cross coupling with 1-iodo-4-nitrobenzene. In all cases, the yields were reasonable to good, and the stable products could be isolated pure by column chromatography.

2.2. *Electronic Absorption Properties.* UV/VIS Spectroscopic analysis of g-DEEs was performed in $CHCl_3$ solutions at room temperature. The effects of donor substitution in g-DEE **4b** show an intense absorption band at λ_{max} 325 nm, whereas g-DEE **3b** with an electron-withdrawing group shows a red-shifted λ_{max} 354 nm (*Fig. 1*). Empirically, D – A-disubstituted g-DEE **5** appears as a more highly colored orange solid in comparison to **3a**,**b** and **4a**,**b** which are all yellowish. The deeper color of **5** is suggestive of a D – A intramolecular charge-transfer (ICT) in the ground state, and the UV/VIS spectrum of **5** shows an absorption tail extending out beyond 400 nm, in addition to a strong absorption at λ_{max} 325 nm (*Fig. 1*). The electronic behavior of this series of g-DEEs is markedly different from that observed in linearly conjugated enynes, for which the 'push-pull' effect of donors and acceptors gives rise to a more substantial red-shift in λ_{max} values [5][18][19]. Obviously, cross-conjugation reduces the extent of electronic communication dramatically.

In the UV/VIS spectra of ferrocenyl-substituted g-DEEs **6** – **8** (*Fig. 2*), a signature broad, weak absorption band spanning from 380 – 550 nm is observed due to the ferrocenyl group, and compounds **6** – **8** show virtually superimposable UV/VIS-absorption profiles in this range (380 – 500 nm). In the higher-energy region, donor-

Scheme. *Synthesis of D/A g-DEEs*

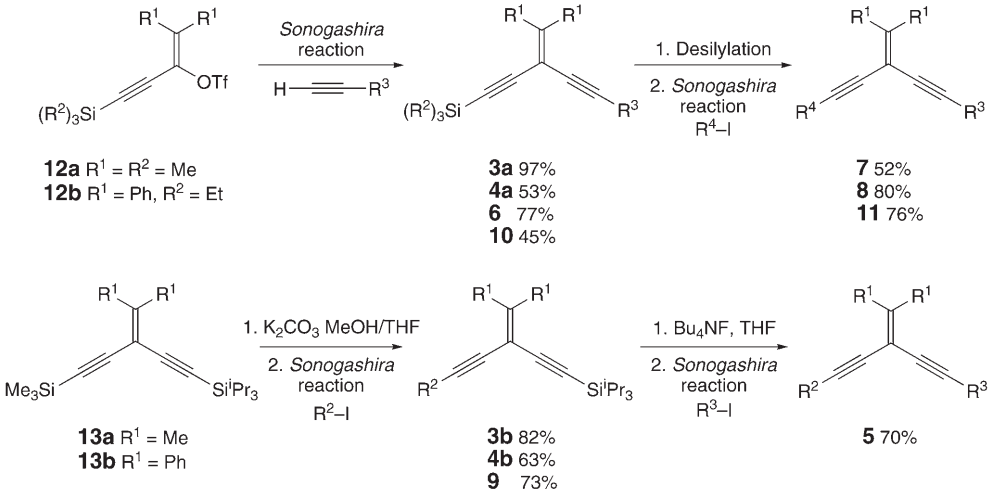

12a $R^1 = R^2 = Me$
12b $R^1 = Ph$, $R^2 = Et$

3a 97%
4a 53%
6 77%
10 45%

7 52%
8 80%
11 76%

13a $R^1 = Me$
13b $R^1 = Ph$

3b 82%
4b 63%
9 73%

5 70%

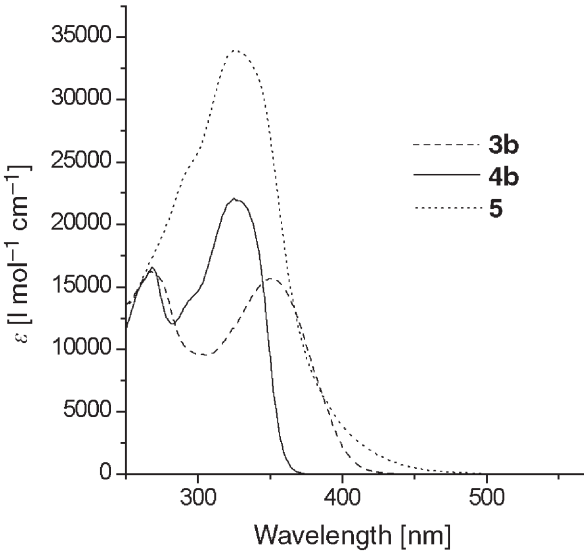

Fig. 1. *UV/VIS Spectra* ($CHCl_3$) *of compounds* **3b**, **4b** *and* **5**

substituted **7** shows a more significant absorption at 330 nm than **6**, similar to that of **4b**. Since ferrocenyl is a π-donor group, the reddish-brown compound **8** is a D – A analogue to compound **5**, and **8** shows a low-energy ICT absorption band at λ_{max} 352 nm.

The π-framework of g-DEEs **9** – **11** is longer than that of compounds **3** – **5** as a result of the pendent phenyl rings. As such, the UV/VIS-spectroscopic features of **9** – **11** (*Fig. 3*) are dominated by a strong absorption in the range of 380 nm for each

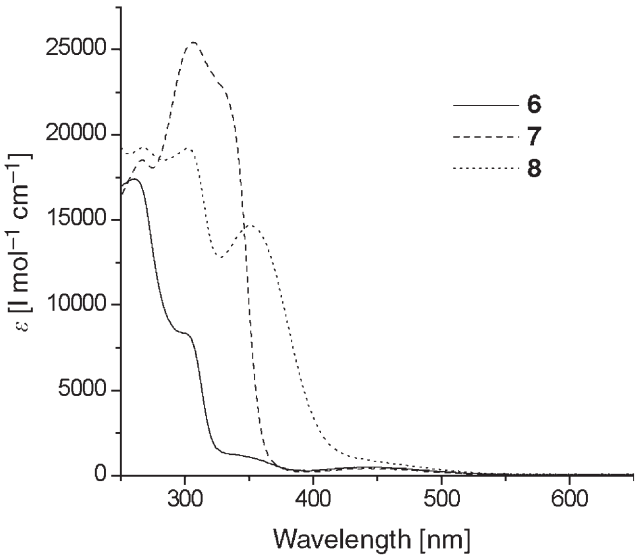

Fig. 2. *UV/VIS Spectra* ($CHCl_3$) *of compounds* **6**, **7**, *and* **8**

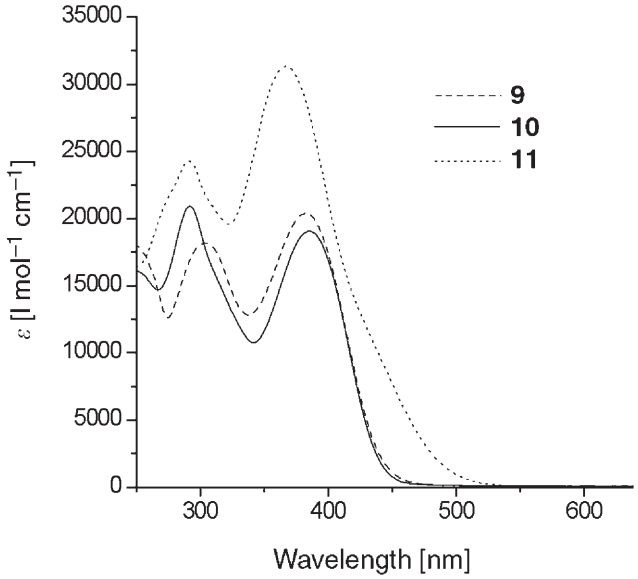

Fig. 3. *UV/VIS Spectra* ($CHCl_3$) *of compounds* **9**, **10** *and* **11**

compound, as found for iso-PDAs **2** [10]. The absorption profile of D – A **11** does, however, show a distinctive shoulder band that appears at 425 nm and indicates ICT between the donor and acceptor moieties *via* the cross-conjugated π-linkage.

2.3. *X-Ray Single-Crystal Structure Analyses.* The solid-state structures of compounds **3b**, **4b**, **7**, and **8** were established by single-crystal X-ray analysis, and the ORTEP plots are drawn in *Fig. 4*. The crystal structure of **3b** (*Fig. 4*,*a*) shows a predominantly planar conjugated framework, with the benzene ring rotated only slightly out of the plane of the enediyne segment by 10.44(10)°. The strongly electron-withdrawing nitrophenyl group, in conjugation with the enediyne backbone, exerts little influence on the observed bond lengths. The alkyne bond lengths of C(1)–C(2) and C(7)–C(8) are comparable to the other derivatives of this study (*Table 1*), as well as to other cross-conjugated enediynes [10][17][20–23]. The alkylidene bond angle C(2)–C(3)–C(7) of 117.80(14)° is, however, one of the largest observed to date for g-DEE structures. Also of note is a rather substantial bending found for the bond angle Si–C(1)–C(2) of 171.88(14)°, which demonstrates the inherent flexibility that alkynyl bonds often show in the solid state [24].

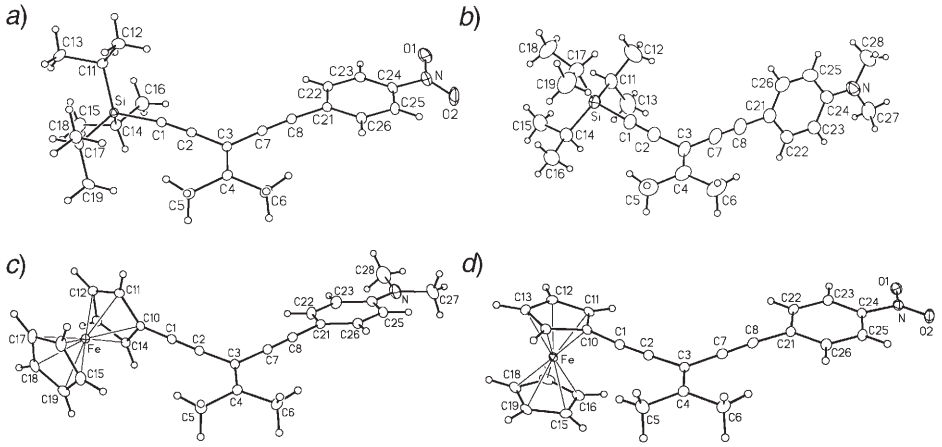

Fig. 4. *ORTEP Drawings of* a) **3b**, b) **4b** (molecule *A*), c) **7**, *and* d) **8** (all at 20% probability level)

Table 1. *Selected Bond Lengths and Angles for* **3b**, **4b**, **7**, *and* **8**

		3b	**4b**[a])	**4b**[b])	**7**	**8**
Bond length [Å]:	C(1)–C(2)	1.211(2)	1.200(3)	1.200(3)	1.196(2)	1.201(4)
	C(7)–C(8)	1.196(2)	1.193(4)	1.182(4)	1.195(3)	1.187(4)
	C(8)–C(21)	1.439(2)	1.433(4)	1.434(4)	1.432(3)	1.438(4)
	C(3)–C(4)	1.362(2)	1.335(4)	1.339(4)	1.348(2)	1.355(4)
Bond angle [°]:	Si–C(1)–C(2) or C(10)–C(1)–C(2)	171.88(14)	177.6(3)	175.7(3)	178.16(18)	175.9(3)
	C(1)–C(2)–C(3)	176.82(17)	178.3(3)	178.5(3)	176.10(18)	178.6(3)
	C(2)–C(3)–C(7)	117.80(14)	114.6(3)	116.5(3)	114.05(15)	116.6(2)
	C(3)–C(7)–C(8)	177.52(19)	178.4(3)	179.3(3)	176.07(18)	178.2(3)
	C(7)–C(8)–C(21)	176.42(19)	178.4(3)	177.6(3)	177.58(17)	175.4(3)

[a]) Crystallographic molecule *A*. [b]) Crystallographic molecule *B*.

Two crystallographically independent molecules are found in the unit cell of **4b**, and the structure of molecule *A* is shown in *Fig. 4,b*. The cross-conjugated enediyne skeletons of molecules *A* and *B* both adopt a similar planar geometry, whereas the dihedral angle between the benzene-ring plane and the enediyne plane differ considerably between the two structures. In molecule *A*, the benzene-ring plane rotates from the enediyne plane by 71.56(11)°, while this value is only 10.5(2)° in molecule *B*. The twisting likely results simply from crystal-packing forces. The olefinic C(3)–C(4) and alkyne bond lengths show no significant variation between the two structures. The enediyne alkylidene angles C(2)–C(3)–C(7) (114.6(3)° for *A* and 116.5(3)° for *B*) are in line with other reported geminal enediynes and the theoretical calculations (*vide infra*).

Ferrocenyl compound **7** (*Fig. 4,c*) shows a nearly orthogonal twisting between the cyclopentadiene (Cp) ring and the enediyne plane in the solid-state structure with a torsional angle of 87.77(7)°. Also, the benzene ring slightly rotates out of the enediyne plane by 20.70(10)°. Bond lengths and angles are, however, unremarkable.

Crystallographic analysis of **8** (*Fig. 4,d*) shows a remarkably planar configuration for the conjugated framework, and the Cp, enediyne, and benzene moieties are all virtually coplanar. Specifically, the benzene ring is twisted from the enediyne plane by only 1.56(19)° and the Cp ring deviates from the enediyne plane by 14.70(16)°. Such a coplanar arrangement supports the prospect of maximum electron delocalization by means of π-orbital overlap. Also interesting is the packing of **8**, which assumes a noncentrosymmetric geometry of the monoclinic $P2_1$ (No. 4) space group, with the major dipole component aligned approximately along the *b*-axis, as shown in *Fig. 5*. It has been shown that this anisotropic feature favors maximal bulk second-order nonlinear optical susceptibility ($\chi^{(2)}$) in the solid state [25].

2.4. *Third-Order Nonlinear Optical* (NLO) *Measurements.* The oligomers of cross-conjugated iso-poly(diacetylenes) have shown interesting third-order NLO properties as a function of length [10]. To complement these results, an understanding of the impact of D/A functionalization on their third-order NLO behavior is needed, especially in comparison to related molecules such as DEEs and tetraethynylethenes (TEEs) [3][7]. The third-order NLO response of various D/A-functionalized g-DEEs was measured by the differential optical *Kerr* effect (DOKE) technique [26] at 800 nm (far from resonance). Samples of g-DEEs **3**–**11** were prepared in THF solution with concentrations of 0.10–0.35M. *Table 2* summarizes the second molecular hyperpolarizabilities, γ, and selected two-photon-absorption (TPA) cross-sections, $\sigma^{(2)}$, in comparison to the unsubstituted g-DEE derivative **14**, TEEs **15** and **16**, and DEEs **17** [3][2]).

Several trends can be seen from this data. First, it is evident that donor/acceptor-substituted g-DEEs **3**–**11** show an increased NLO response compared to unsubstituted g-DEE **14**. This is not unexpected, as it has been well established that an increase in γ can be achieved through increasing the level of static polarization within a molecule.

---

[2]) It is, unfortunately, difficult to compare the absolute γ-values for molecules measured by different methods (*i.e.*, THG (third-harmonic generation) *vs.* DOKE). We, therefore, concentrate our discussion on general trends in the observed values.

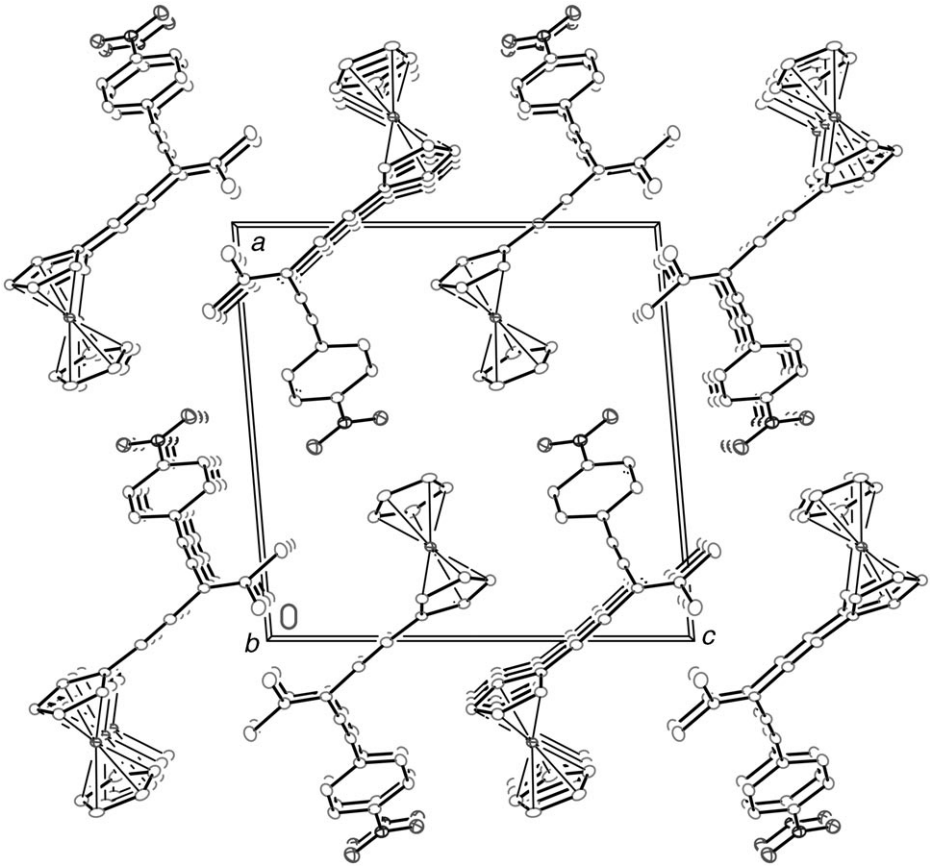

Fig. 5. *Crystal packing of compound* **8**

The sole anomaly to this trend is the electron-rich derivative **7**, for which a relatively low value of $\gamma = 3 \cdot 10^{-36}$ esu was obtained. While the origin of this low value is not empirically obvious, theoretical analysis does potentially shed some light on this behavior (*vide infra*). Second, the γ-values of acceptor-substituted g-DEEs (see **3a** and **9**) are consistently higher than those of their donor-substituted g-DEEs analogues (see **4a** and **10**). This contrasts those observed for linearly conjugated TEEs **15a** *vs.* **15b** for which the γ-value of **15b** is nearly three times that of **15a**, and those found for linearly conjugated DEEs, where bis-donor **17b** ($\gamma = 300 \cdot 10^{-36}$ esu) shows a superior response to bis-acceptor **17a** ($\gamma = 210 \cdot 10^{-36}$ esu). Finally, D – A-type g-DEEs **5**, **8**, and **11** all show greater γ-values than either mono-D- or mono-A-type g-DEEs, demonstrating that electronic interactions between D – A groups can affect the molecular second hyperpolarizabilities through a 'push-pull' electronic structure. This contrasts the behavior of g-TEEs **16a** – **c**, where the D – A molecule **16c** shows the lowest value of any of the TEE derivatives. The difference in behavior between the TEE **16c** *vs.* g-DEEs **5**, **8**, and **11** may derive from the fact that the TEE core itself is known to be a strong

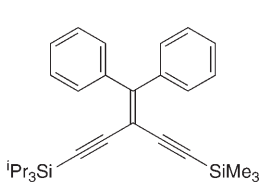

14

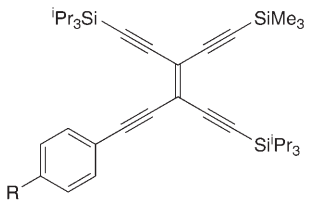

15a R = NO_2
15b R = NMe_2

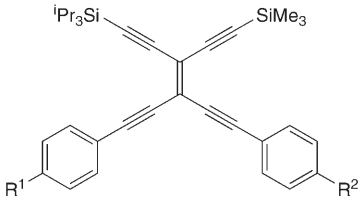

16a $R^1 = R^2 = OMe$
16b $R^1 = R^2 = NMe_2$
16c $R^1 = NMe_2$, $R^2 = NO_2$

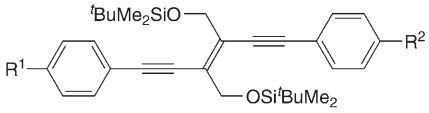

17a $R^1 = R^2 = NO_2$
17b $R^1 = R^2 = NMe_2$
17c $R^1 = NMe_2$, $R^2 = NO_2$

Table 2. *Molecular Second Hyperpolarizabilities* (γ) *and Selected Two-Photon-Absorption Cross-Sections* ($\sigma^{(2)}$) *for* **3**–**17**

Compound	γ [10^{-36} esu]	$\sigma^{(2)}$ [GM]	Type of D/A substitution
3a	23 ± 2[a])		acceptor – g-DEE
3b	16 ± 2[a])		acceptor – g-DEE
4a	14 ± 2[a])		donor – g-DEE
5	28 ± 3[a])	6 ± 1[b])	donor – g-DEE – acceptor
6	15 ± 12[a])[c])		donor – g-DEE
7	3 ± 8[a])[d])		donor – g-DEE – donor
8	35 ± 9[a])		donor – g-DEE – acceptor
9	29 ± 2[a])	12 ± 2[b])	acceptor – g-DEE
10	15 ± 1[a])	18 ± 3[b])	donor – g-DEE
11	37 ± 3[a])	22 ± 4[b])	donor – g-DEE – acceptor
14	9.2 ± 0.4[a])		not applicable
15a	95[e])		acceptor – TEE
15b	270[e])		donor – TEE
16a	130[e])		donor – g-TEE – donor
16b	310[e])		donor – g-TEE – donor
16c	59[e])		donor – g-TEE – acceptor
17a	210[e])		acceptor – DEE – acceptor
17b	300[e])		donor – DEE – donor
17c	610[d])		donor – DEE – acceptor

[a]) Referenced to THF ($\gamma_{THF} = 5.2 \cdot 10^{-37}$ esu), see [26]. [b]) Referenced to MPPBT ($\sigma^{(2)} = 380$ GM), see [27]. [c]) The sample displayed unexplained absorption and/or scattering during DOKE analysis resulting in a larger level of uncertainty compared to other samples. [d]) The sample displayed incomplete solubility at the concentration used for NLO measurements. Thus, the γ-value represents a minimum value only and contains a large level of uncertainty. [e]) Measured by THG at 1.9 μm, see [3].

electron acceptor[3]), and this may moderate the D–A interaction of the pendent substituents of **16c** and result in a lower overall polarization. It can also be noted that the largest γ-value observed in the current study – that of D–A g-DEE **11** – is likely higher than that of D–A g-DEEs **8** and **5** because **11** possesses a longer linearly-conjugated π-delocalization, due to the pendent phenyl rings.

In addition to the measurement of γ, the DOKE setup used in this study also allows for the concurrent assessment of the two-photon-absorption (TPA) cross-section ($\sigma^{(2)}$) of the samples under study at 800 nm [30]. Several samples, *i.e.*, **5** and **9**–**11**, were therefore examined, and, while modest, the TPA cross-section does show an increase in $\sigma^{(2)}$ from 6 to 12 GM upon changing from an acceptor (see **9**) to a donor g-DEE (see **10**), and a further increase in $\sigma^{(2)}$ to 22 GM is found for the D–A g-DEE **11**. The more highly conjugated D–A g-DEE **11** also shows a superior $\sigma^{(2)}$ to that of D–A g-DEE **5**.

2.5. *Theoretical Evaluation of Electron Delocalization along the Cross-Conjugated g-DEE Backbone.* Electronic communication has been shown experimentally as well as theoretically to be present in cross-conjugated oligomers with g-DEEs as the repeat unit [7–10]. Theoretically, the g-DEE structure represents a challenge to classical resonance theory that predicts that electron delocalization should not be permitted between the two cross-conjugated moieties [31]. Such discrepancies with our experimental results are due to the omission of the weak orbital interactions of π- and σ-bonding and antibonding orbitals in simplified theoretical models. The use of *ab initio* and density-functional-theory (DFT) calculations, however, can help to solve this problem by taking into account these weak interactions. This is especially true using a combination of DFT and natural-bond-orbital (NBO) analysis [32], which are reported to be effective in assessing the electron-delocalization properties of linearly conjugated and cross-conjugated geminal enediynes [33]. In general, the localized (bonding) structure of g-DEEs can be expressed by three terms: the two sets of orthogonal π-orbitals, denoted $\pi_\perp$ and $\pi_{||}$ (*Fig. 6*), as well as the in-plane σ-orbitals, denoted $\sigma_{||}$. As for the electron delocalization, the corresponding antibonding orbitals, $\pi^*_\perp$, $\pi^*_{||}$, and $\sigma^*_{||}$, are thus regarded as the three most significant participants (acceptors). By applying the NBO analysis, first proposed by *Weinhold* [32], it is possible to evaluate the contribution of each set of orbitals to the total electron-delocalization energy.

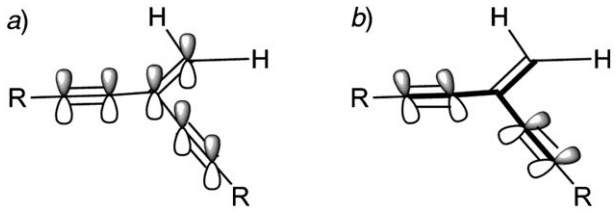

Fig. 6. *Schematic illustration of orbitals in g-DEEs. a*) Out-of-plane (vertical) p-orbitals (denoted $\pi_\perp$), *b*) in-plane p-orbitals (denoted $\pi_{||}$) and σ-bonds (highlighted in bold, denoted $\sigma_{||}$).

DFT Calculations on g-DEE molecules by *Lüthi* and co-workers have indicated that the stability of an unsubstituted g-DEE is primarily controlled by the vertical π-

[3]) For a theoretical analysis of the electron-deficient nature of the DEE backbone, see [28], and for experimental studies, see [29].

delocalization, while the σ-delocalization (*i.e.*, hyperconjugation) has a relatively insignificant role [33]. For D/A-substituted g-DEEs, both π*- and σ*-antibonding orbitals are likely subject to substantial changes according to the substituent groups. To further understand the D/A effects, the delocalization energy (E_{del}) of the g-DEE framework was calculated as a semi-quantitative measure to assess the degree of electron delocalization. For clarity, we herein ascribe the D/A substituents as the external perturbations, and only the delocalization energies contributed by the antibonding orbitals on the g-DEE structure were calculated by using the method reported by *Lüthi* and co-workers [33]. A series of compounds **18a**–**e** representing D- and/or A-functionalized g-DEEs were chosen for the investigation. The molecular structures of **18a**–**e** were first optimized by using DFT methods at the B3LYP/6-31G* level. Frontier-molecular-orbital energies and dipole moments are reported in *Table 3*. NBO Analysis was subsequently performed based on the optimized molecular structures at the same level. For detailed analysis, the total delocalization energy (E_{del}) due to the enediyne backbone is broken down into three components: *a*) the in-plane π*-contribution, $E_{\pi^*\|}$, *b*) the σ*-contribution, $E_{\sigma^*\|}$, and *c*) the out-of-plane (vertical) π*-contribution, $E_{\pi^*\perp}$.

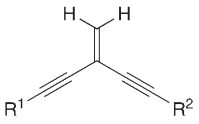

18a R^1 = 4-nitrophenyl, R^2 = H
18b R^1 = 4-aminophenyl, R^2 = H
18c R^1 = R^2 = 4-aminophenyl
18d R^1 = R^2 = 4-nitrophenyl
18e R^1 = 4-nitrophenyl, R^2 = 4-aminophenyl
18f R^1 = R^2 = H

Table 3. *Frontier-Molecular-Orbital Energies and Dipole Moments for* **18a**–**e**, *Calculated at the B3LYP/6–31G* Level*

	HOMO [Hartree]	LUMO [Hartree]	Band gap [Hartree]	Dipole moment [D]
18a	– 0.238	– 0.100	0.138	5.06
18b	– 0.192	– 0.044	0.148	3.29
18c	– 0.182	– 0.042	0.140	3.61
18d	– 0.240	– 0.109	0.131	5.16
18e	– 0.199	– 0.095	0.104	7.68

Table 4 lists the different contributions to delocalization energies due to the three aforementioned components, as well as the total delocalization energies (E_{del}, calculated by deletion of all antibonding and *Rydberg* orbitals) for the series of the g-DEEs **18a**–**e** calculated by NBO analysis at the B3LYP/6-31G* level. Overall, the in-plane σ*-orbitals contribute more significantly to the total delocalization energy than do the in-plane and out-of-plane π*-orbitals. This suggests that hyperconjugative

effects through σ-bonds play a larger role in stabilizing the g-DEE structure than π-electron interactions such as homoconjugation that have been suggested previously [34]. The remarkably large delocalization energies for D–A-type **18e** supply evidence for enhanced D–A electronic interactions *via* the enediyne backbone, which is in accordance with the conclusions of the UV/VIS analysis (*vide supra*). The $E_{\pi^*||}$ values for monosubstituted g-DEEs **18a** and **18b** are comparable to that of an unsubstituted g-DEE reported by *Lüthi* and co-workers [33], while the $E_{\pi^*\perp}$ values are greater than that of the unsubstituted g-DEE. For the disubstituted g-DEEs **18c–e**, each delocalization contributor as well as the total delocalization energy increases although the total delocalization energy for D–D-type **18c** shows only a slight increase relative to mono-D-type **18b**. Such a low total delocalization energy could disfavor charge separation in the excited state, and the change of dipole moments ($\Delta\mu$) between the ground and excited states could be small. Given that $\Delta\mu$ is considered an important factor governing the third-order NLO susceptibility, this may explain the observation that D–D g-DEE gives the smallest second-order hyperpolarizability γ (*vide supra*).

Table 4. *Delocalization Energies Contributed by In- and Out-of-Plane Orbitals on D/A Substituted g-DEEs* **18a–e**

	$E_{\pi^*\|\|}$ [kcal/mol]	$E_{\sigma^*\|\|}$ [kcal/mol]	$E_{\pi^*\perp}$ [kcal/mol]	total E_{del}[a]) [kcal/mol]	D/A type
18a	15.537	133.031	62.886	1062.238	mono-A
18b	10.652	136.691	55.754	763.286	mono-D
18c	20.973	141.828	87.656	1251.422	D–D
18d	21.189	141.037	79.880	1905.480	A–A
18e	21.185	141.454	84.368	1552.758	D–A
18f[b])	10.49	159.29	48.43	not available	

[a]) E_{del} is the total delocalization energy calculated by deleting all antibonding orbitals, including those of the aryl substituent(s). [b]) Values from [33].

Nevertheless, to assess the influence of D/A groups on electron delocalization along the enediyne backbone, it seems more meaningful to look at the delocalization-energy (E_{del}) differences between each pair of D/A compounds as shown in *Table 5*. The contribution of vertical π^*-orbitals ($\pi^*_\perp$) is consistently larger than those of the in-plane contributors ($\pi^*_{||}$), indicating that these π^*-bonds are more sensitive to the influence of terminal groups.

Table 5. *Energy Differences between D/A Substituted g-DEEs*

	$\Delta E_{\pi^*\|\|}$ [kcal/mol]	$\Delta E_{\sigma\|\|}$ [kcal/mol]	$\Delta E_{\pi^*\perp}$ [kcal/mol]
18d–18a (AA–A)	5.652	8.006	16.994
18c–18b (DD–D)	10.321	5.137	31.902
18e–18b (DA–D)	10.533	4.763	28.614
18e–18a (DA–A)	5.648	8.428	21.482

Another approach to evaluate the delocalization properties of g-DEEs is to assess the bond-length-alternation (BLA) index, δR. In general, the BLA index for the cross-conjugated enynes is defined by *Eqn. 1*, where the C_D-C_T, $C_{Ar}-C_T$, C=C, and C≡C

refer to the average bond distances for each type of single or multiple bond, respectively [8]. The δR values for each type of g-DEE (*Table 6*) obtained from DFT calculations show that δR decreases monotonically from **18a** to **18e** and suggest that the degree of delocalization in the enediyne backbone tends to increase as more D/A chromophores are appended. Experimental results from the X-ray structural analysis also show a consistent trend where δR values decrease as the degree of substitution is increased, with the exception of compound **3d**. Given the range of geometries found in the solid state, however, the observed trend is also quite possibly fortuitous.

$$\delta R = (C_D - C_T + C_{Ar} - C_T)/2 - (C{=}C + C{\equiv}C)/2 \quad (1)$$

Table 6. *BLA Indexes δR for g-DEEs*

	δR [Å]	
	theoretical[a])	experimental[b])
18a	0.145	0.158 (from **3d**)
18b	0.144	0.173 (from **3b**)
18c	0.142	not available
18d	0.141	0.161 (from **4c**)
18e	0.140	0.159 (from **4b**)

[a]) Based on DFT calculations. [b]) Based on X-ray crystallographic analysis.

3. Conclusion. – A series of D/A functionalized g-DEEs was prepared by Pd-catalyzed coupling reactions and their solid-state structural properties investigated by single-crystal X-ray analysis. Electronic absorption spectroscopic analysis suggests an ICT band in the spectra of D–A-functionalized g-DEEs **5**, **8**, and **11**, consistent with electronic communication through the geminal enediyne framework. Ultrafast third-order NLO properties for this g-DEEs series were evaluated by the DOKE detection technique in THF solutions. The donor–acceptor motifs for **5**, **8**, and **11** yield the largest second hyperpolarizability (γ) values of the series, whereas donor-substituted g-DEEs appear to show the weakest response. A theoretical study using NBO analysis shows that the contributions of π*- and σ*-bonds to the electron delocalization along the geminal enediyne backbone vary with the nature of substituents. The vertical π*-orbitals are most susceptible to influences that arise from pendent functionalization. Overall, the joint experimental and theoretical studies may serve as a useful guide for the chemical functionalization of molecular materials in efforts to tune electronic and nonlinear optical properties.

This research was supported by the University of Alberta, the *Natural Sciences and Engineering Research Council of Canada* (*NSERC*), *ASRA*, *CIPI*, *iCORE*, and *Petro-Canada* (*Young Innovator Award* to *R. R. T.*). We thank Dr. *Hans Peter Lüthi* and *Peter Limacher* for helpful discussions for the NBO analysis.

Experimental Part

General. All chemicals were purchased from *Aldrich* and used without further purification. THF was dried over sodium/benzophenone and distilled under N_2 prior to use. Column chromatography (CC): silica gel *60* (230–400 mesh) from *General Intermediates of Canada*. Thin layer chromatography (TLC): aluminum sheet coated with silica gel *60* F_{254} from *Whatman*; visualization by UV light or $KMnO_4$ stain. Melting point: *Fisher–Johns* or *Gallenkamp* apparatus; uncorrected. UV/VIS Spectra: *Varian Cary 400* at r.t.; λ in nm (ε in l mol^{-1} cm^{-1}). IR Spectra: *Nicolet Magna-IR 750* (neat) or *Nic-Plan IR Microscope* (solids); in cm^{-1}. ^{1}H- and ^{13}C-NMR Spectra: *Varian Gemini-300*, *-400*, or *-500* and *Bruker AM-300* instruments; at r.t. in $CDCl_3$; δ in ppm with solvent peaks (δ 7.24 for ^{1}H and 77.0 for ^{13}C) as reference, *J* in Hz; for simplicity, the coupling constants of aromatic protons of 4-substituted phenyl groups are reported as pseudo-first-order, even though they are second-order spin (*AA′BB′*) systems. EI-MS: *Kratos MS-50* instrument in *m*/*z*; low-resolution data are provided in cases when M^+ is not the base peak; otherwise, only high-resolution data is provided. Elemental analyses were performed by the Microanalytical Service, Department of Chemistry, University of Alberta.

Cross-Coupling: General Procedure (*G. P.*). A mixture of the appropriate (trimethylsilyl)- or (triisopropylsilyl)-protected alkyne and K_2CO_3 (*ca.* 0.2 equiv.) or Bu_4NF (1.1 equiv.) in wet THF/MeOH 10 : 1 (20 ml) or THF (20 ml), respectively, was stirred at r.t. until TLC analysis showed that desilylation was complete (typically < 2 h). Et_2O and sat. aq. NH_4Cl soln. were added, the org. phase was washed with sat. aq. NH_4Cl soln. (2×50 ml), dried, concentrated to *ca.* 3 ml, and added to a deoxygenated soln. of the vinyl triflate or aryl halide coupling partner in THF or DMF (20 ml). $[Pd(PPh_3)_4]$ or $[PdCl_2(PPh_3)_2]$ (*ca.* 0.05 equiv.) and $^iPr_2NH$ or Et_2NH were sequentially added, the soln. was stirred for 5 min, CuI (*ca.* 0.15 equiv.) was added, and the soln. was stirred until TLC analysis no longer showed the presence of the deprotected alkyne starting material. Et_2O and H_2O were added, the org. phase was separated, washed with sat. aq. NH_4Cl (2×50 ml), dried, and concentrated. Flash CC gave the desired product.

4-Methyl-3-[(4-nitrophenyl)ethynyl]-1-(trimethylsilyl)pent-3-en-1-yne (**3a**). According to the *G. P.*, with 1-nitro-4-[(trimethylsilyl)ethynyl]benzene (100 mg, 0.502 mmol) and K_2CO_3 (60 mg, 0.4 mmol) in wet THF (5 ml) and MeOH (25 ml), then with vinyl triflate **12a** [16] (150 mg, 0.500 mmol), deoxygenated THF (30 ml), $^iPr_2NH$ (5 ml), $[Pd(PPh_3)_4]$ (18 mg, 0.016 mmol), and CuI (9 mg, 0.047 mmol) for 1 h. CC (silica gel, hexane/Et_2O 3 : 1) afforded **3a** (144 mg, 97%). Bright yellow solid. M.p. 66–67°. R_f 0.72 (hexane/Et_2O 3 : 1). IR (microscope): 3079, 2957, 2204, 2150, 1511, 1341. ^{1}H-NMR (400 MHz, $CDCl_3$): 8.15 (*d*, *J* = 9.2, 2 H); 7.56 (*d*, *J* = 8.8, 2 H); 2.09 (*s*, 6 H); 0.21 (*s*, 9 H). ^{13}C-NMR (100 MHz, APT, $CDCl_3$): 158.1; 146.8; 132.0; 130.4; 123.5; 101.2; 100.7; 97.0; 91.6; 89.6; 23.0; 22.9; −0.06. EI-MS: 297.1 (94, M^+), 282.1 (100, $[M - Me]^+$). HR-MS: 297.1191 ($C_{17}H_{19}NO_2Si^+$; calc. 297.1185).

4-Methyl-3-[(4-nitrophenyl)ethynyl]-1-(triisopropylsilyl)pent-3-en-1-yne (**3b**). According to the *G. P.*, with **13a** (256 mg, 0.770 mmol) [17] and K_2CO_3 (58 mg, 0.42 mmol) in wet THF (5 ml) and MeOH (25 ml), then with 1-iodo-4-nitrobenzene (187 mg, 0.751 mmol), deoxygenated Et_3N (50 ml), $[PdCl_2(PPh_3)_2]$ (21 mg, 0.03 mmol), and CuI (6 mg, 0.030 mmol) for 19 h. CC (silica gel, hexane/CH_2Cl_2 3 : 1) afforded **3b** (240 mg, 82%). Bright yellow solid. M.p. 70–72°. R_f 0.32 (hexane/CH_2Cl_2 3 : 1). UV/VIS ($CHCl_3$): 268 (16200), 351 (15600). IR (CH_2Cl_2, cast): 2942, 2865, 2206, 2148, 1592, 1520, 1343. ^{1}H-NMR (300 MHz, $CDCl_3$): 8.16 (*d*, *J* = 8.8, 2 H); 7.54 (*d*, *J* = 8.8, 2 H); 2.11 (*s*, 3 H); 2.10 (*s*, 3 H); 1.10 (*s*, 21 H). ^{13}C-NMR (75.5 MHz, $CDCl_3$): 157.2; 146.9; 132.0; 130.6; 123.6; 102.8; 101.7; 93.6; 92.1; 89.5; 23.1; 23.0; 18.7; 11.4. EI-MS: 381.2 (27, M^+), 338.2 (100, $[M - {}^iPr]^+$). HR-MS: 381.2115 ($C_{23}H_{31}NO_2Si^+$; calc. 381.2124). Anal. calc. for $C_{23}H_{31}NO_2Si$: C 72.39, H 8.19, N 3.67; found: C 72.20, H 8.20, N 3.63.

3-{[4-(Dimethylamino)phenyl]ethynyl}-4-methyl-1-(trimethylsilyl)pent-3-en-1-yne (= N,N-*Dimethyl-4-{4-methyl-3-[(trimethylsilyl)ethynyl]pent-3-en-1-ynyl}benzenamine*; **4a**). According to the *G. P.*, with 4-ethynyl-*N*,*N*-dimethylbenzenamine (66 mg, 0.46 mmol), vinyl triflate **12a** [16] (215 mg, 0.683 mmol), deoxygenated THF (10 ml), Et_3N (10 ml), $[PdCl_2(PPh_3)_2]$ (16 mg, 0.023 mmol), and CuI (9 mg, 0.047 mmol) overnight. CC (silica gel, hexane/CH_2Cl_2 4 : 1) afforded **4a** (72 mg, 53%). Colorless oil. R_f 0.62 (hexanes/CH_2Cl_2 1 : 1). UV/VIS (CH_3Cl): 266 (15100), 294 (sh, 14100), 324 (19200). IR (KBr): 2962, 2925, 2902, 2849, 2198, 2144, 1609, 1523, 1446. ^{1}H-NMR (500 MHz, $CDCl_3$): 7.34 (*d*, *J* = 8.5, 2 H); 6.62 (*d*, *J* = 8.5, 2 H); 2.97 (*s*, 6 H); 2.08 (*s*, 3 H); 2.07 (*s*, 3 H); 0.22 (*s*, 9 H). ^{13}C-NMR (125 MHz,

$CDCl_3$): 153.8; 150.0; 132.5; 111.8; 110.5; 102.2; 101.9; 95.6; 92.4; 84.0; 40.2; 22.72; 22.68; 0.09. HR-EI-MS: 295.1753 ($C_{19}H_{25}NSi^+$, M^+; calc. 295.1756).

3-{[4-(Dimethylamino)phenyl]ethynyl}-4-methyl-1-(triisopropylsilyl)pent-3-en-1-yne (= N,N-*Dimethyl-4-{4-methyl-3-[(triisopropylsilyl)ethynyl]pent-3-en-1-ynyl}benzenamine*; **4b**). According to the *G. P.*, with **13a** (325 mg, 0.979 mmol) [17] and K_2CO_3 (50 mg, 0.36 mmol) in wet THF (5 ml) and MeOH (25 ml), then with 4-iodo-*N,N*-dimethylbenzenamine (250 mg, 1.01 mmol), deoxygenated Et_3N (50 ml), [$PdCl_2(PPh_3)_2$] (59 mg, 0.084 mmol), and CuI (31 mg, 0.16 mmol) for 20 h. CC (silica gel *H*, hexane/CH_2Cl_2 3:1) afforded **4b** (229 mg, 63%). Pale yellow solid. M.p. 45–46°. R_f 0.31 (hexane/CH_2Cl_2 2:1). UV/VIS ($CHCl_3$): 268 (16500), 302 (sh, 15000), 325 (21000). IR (neat): 2942, 2865, 2202, 2150, 1607, 1521, 1366. ^{1}H-NMR (300 MHz, $CDCl_3$): 7.31 (*d*, *J* = 9.0, 2 H); 6.61 (*d*, *J* = 9.0, 2 H); 2.95 (*s*, 6 H); 2.063 (*s*, 3 H); 2.059 (*s*, 3 H); 1.09 (*s*, 21 H). ^{13}C-NMR (75.5 MHz, $CDCl_3$): 152.8; 150.0; 132.5; 111.9; 110.7; 104.2; 102.5; 92.3; 92.0; 84.5; 40.3; 22.8; 22.7; 18.8; 11.4. EI-MS: 379 (100, M^+). HR-MS: 379.2700 ($C_{25}H_{37}NSi^+$; calc. 379.2695).

3-{[4-(Dimethylamino)phenyl]ethynyl}-4-methyl-1-(4-nitrophenyl)pent-3-en-1-yne (= N,N-*Dimethyl-4-{4-methyl-3-[(4-nitrophenyl)ethynyl]pent-3-en-1-ynyl}benzenamine*; **5**). According to the *G. P.*, with **4b** (70 mg, 0.18 mmol) and 1M Bu_4NF in THF (0.7 ml) in wet THF (20 ml), then with 1-iodo-4-nitrobenzene (48 mg, 0.19 mmol), deoxygenated Et_3N (20 ml), THF (20 ml), [$PdCl_2(PPh_3)_2$] (5 mg, 0.007 mmol), and CuI (3 mg, 0.02 mmol) for 12 h. CC (silica gel *H*, hexane/CH_2Cl_2 1:1) afforded **5** (44 mg, 70%). Orange solid. M.p. 159–162°. R_f 0.45 (hexane/AcOEt 3:1). UV/VIS ($CHCl_3$): 302 (sh, 26300), 325 (34000). IR (CH_2Cl_2, cast): 2903, 2198, 1607, 1518, 1341. ^{1}H-NMR (300 MHz, $CDCl_3$): 8.16 (*d*, *J* = 9.0, 2 H); 7.59 (*d*, *J* = 9.0, 2 H); 7.35 (*d*, *J* = 8.9, 2 H); 6.63 (*d*, *J* = 8.9, 2 H); 2.97 (*s*, 6 H); 2.143 (*s*, 3 H); 2.137 (*s*, 3 H). ^{13}C-NMR (75.5 MHz, $CDCl_3$): 154.9; 150.2; 146.8; 132.6; 132.1; 130.7; 123.6; 111.9; 110.0; 101.5; 93.1; 92.6; 89.2; 83.6; 40.3; 23.03; 23.01. HR-EI-MS: 344.1522 ($C_{22}H_{20}N_2O_2$, M^+; calc. 344.1525).

4-Methyl-3-(ferrocenylethynyl)-1-(trimethylsilyl)pent-3-en-1-yne (= *1-{4-Methyl-3-[(trimethylsilyl)-ethynyl]pent-3-en-1-ynyl}ferrocene*; **6**). According to the *G. P.*, with 1-ethynylferrocene (135 mg, 0.643 mmol), triflate **12a** (193 mg, 0.643 mmol), degassed THF (20 ml), [$PdCl_2(PPh_3)_2$] (22 mg, 0.031 mmol), ^{i}Pr_2NH (2 ml), and CuI (11 mg, 0.058 mmol) for 1.5 h. CC (hexane/CH_2Cl_2 2:1) afforded **6** (178 mg, 77%). Yellow solid. R_f 0.4 (hexane/CH_2Cl_2 2:1). M.p. 66–67°. UV/VIS ($CHCl_3$): 261 (17400), 299 (8400), 341 (1200), *ca.* 447 (500). IR (microscope): 3095, 2960, 2903, 2207, 2146, 1247. ^{1}H-NMR (300 MHz, $CDCl_3$): 4.45 (br. *s*, 2 H); 4.22 (br. *s*, 7 H); 2.04 (*s*, 3 H); 2.03 (*s*, 3 H); 0.20 (*s*, 9 H). ^{13}C-NMR (75.5 MHz, $CDCl_3$, APT): 154.2; 102.2; 102.0; 95.8; 90.2; 82.4; 71.4; 69.9; 68.7; 65.5; 22.8; 0.1 (one coincident signal not observed). HR-EI-MS: 360.0994 ($C_{21}H_{24}FeSi^+$, M^+; calc. 360.0997).

3-{[4-(Dimethylamino)phenyl]ethynyl}-1-ferrocenyl-4-methylpent-3-en-1-yne (= *1-{3-{[4-(Dimethylamino)phenyl]ethynyl}-4-methylpent-3-en-1-ynyl}ferrocene*; **7**). According to the *G. P.*, with **6** (102 mg, 0.28 mmol) and K_2CO_3 (10 mg, 0.14 mmol) in wet THF (5 ml) and MeOH (25 ml), then with 4-iodo-*N,N*-dimethylbenzenamine (74 mg, 0.30 mmol), degassed THF (20 ml), [$PdCl_2(PPh_3)_2$] (10 mg, 0.014 mmol), ^{i}Pr_2NH (2 ml), and CuI (5 mg, 0.03 mmol) for 1.5 h. CC (hexane/Et_2O 5:1) afforded **7** (60 mg, 52%) as a yellow solid. R_f 0.4 (hexane/Et_2O 5:1). M.p. 174–175°. IR ($CHCl_3$, cast): 3084, 2925, 2197, 1612, 1526, 1441, 1369. UV/VIS ($CHCl_3$): 305 (25400), 330 (22600), *ca.* 445 (500). ^{1}H-NMR (300 MHz, $CDCl_3$): 7.34 (*d*, *J* = 8.4, 2 H); 6.62 (*d*, *J* = 8.4, 2 H); 4.45 (*t*, *J* = 1.8, 2 H); 4.21 (*s*, 5 H); 4.18 (*t*, *J* = 1.8, 2 H); 2.96 (*s*, 6 H); 2.08 (*s*, 6 H). ^{13}C-NMR (75.5 MHz, $CDCl_3$, APT): 151.1; 150.0; 132.5; 111.9; 110.6; 102.2; 92.0; 89.6; 84.7; 83.1; 71.4; 69.9; 68.6; 65.8; 40.3; 22.8; 22.7. HR-EI-MS: 407.1350 ($C_{26}H_{25}FeN^+$, M^+; calc. 407.1336).

1-Ferrocenyl-4-methyl-3-[(4-nitrophenyl)ethynyl]pent-3-en-1-yne (= *1-{4-Methyl-3-[(4-nitrophenyl]-ethynyl]pent-3-en-1-ynyl}ferrocene*; **8**). According to the *G. P.*, with **6** (52 mg, 0.14 mmol) and K_2CO_3 (6 mg, 0.04 mmol) in wet THF (5 ml) and MeOH (25 ml), then with 1-iodo-4-nitrobenzene (54 mg, 0.22 mmol), degassed THF (20 ml), [$PdCl_2(PPh_3)_2$] (10 mg, 0.014 mmol), ^{i}Pr_2NH (2 ml), and CuI (5 mg, 0.03 mmol) for 1.5 h. CC (hexane/Et_2O 5:1) afforded **8** (47 mg, 80%). Brown solid. R_f 0.5 (hexane/Et_2O 5:1). M.p. 113–114°. UV/VIS ($CHCl_3$): 302 (19200), 352 (14700). IR (CH_2Cl_2, cast): 3102, 2905, 2845, 2202, 1591, 1516, 1342. ^{1}H-NMR (300 MHz, $CDCl_3$): 8.17 (*d*, *J* = 9.0, 2 H); 7.58 (*d*, *J* = 9.0, 2 H); 4.49 (*s*, 2 H); 4.24 (*s*, 7 H); 2.132 (*s*, 3 H); 2.127 (*s*, 3 H). ^{13}C-NMR (75.5 MHz, $CDCl_3$, APT): 155.5; 146.9; 132.0;

130.6; 123.6; 101.4; 92.3; 90.9; 89.2; 81.8; 71.8; 70.4; 69.4; 65.7; 23.1; 23.0. HR-EI-MS: 409.0768 ($C_{24}H_{19}FeNO_2^+$, M^+; calc. 409.0765).

3-(Diphenylethylidene)-1-(4-nitrophenyl)-5-(triisopropylsilyl)penta-1,4-diyne (**9**). According to the *G. P.*, with **13b** [10] (41 mg, 0.090 mmol) and K_2CO_3 (6 mg, 0.04 mmol) in wet THF (0.5 ml) and MeOH (3 ml), then with 1-iodo-4-nitrobenzene (25 mg, 0.10 mmol), deoxygenated Et_3N (5 ml), [$PdCl_2(PPh_3)_2$] (4 mg, 0.006 mmol), and CuI (2 mg, 0.01 mmol) for 24 h. CC (silica gel *H*, hexane/CH_2Cl_2 3:1) afforded **9** (33 mg, 73%). Yellow solid. M.p. 62–65°. R_f 0.32 (hexane/CH_2Cl_2 2:1). UV/VIS ($CHCl_3$): 304 (18200), 382 (20400). IR ($CHCl_3$, cast): 2941, 2864, 2194, 2147, 1593, 1519, 1342. ^{1}H-NMR (300 MHz, $CDCl_3$): 8.11 (*d*, *J* = 8.8, 2 H); 7.55–7.29 (*m*, 12 H); 1.03 (*s*, 21 H). ^{13}C-NMR (75.5 MHz, $CDCl_3$): 158.2; 146.9; 140.3; 139.8; 132.0; 130.4 (2×); 128.92; 128.89; 127.84; 127.82; 123.6; 104.3; 101.8; 95.9; 94.8; 89.6; 18.7; 11.4 (one coincident signal not observed). HR-EI-MS: 505.2444 ($C_{33}H_{35}NO_2Si^+$, M^+; calc. 505.2437).

1-[4-(Dimethylamino)phenyl]-3-(diphenylethylidene)-1-(triethylsilyl)penta-1,4-diyne (=*4-[3-(Diphenylethylidene)-5-(triethylsilyl)penta-1,4-diynyl]*-N,N-*dimethylbenzenamine*; **10**). According to the *G. P.*, with *N,N*-dimethyl-4-[(trimethylsilyl)ethynyl]benzenamine (100 mg, 0.460 mmol) and K_2CO_3 (20 mg, 0.15 mmol) in wet THF (10 ml) and MeOH (10 ml), then with **12b** (180 mg, 0.386 mmol), deoxygenated DMF (125 ml), [$Pd(PPh_3)_4$] (24 mg, 0.021 mmol), Et_2NH (3 ml), and CuI (13 mg, 0.068 mmol) for 17 h. CC (silica gel, AcOEt/hexanes 1:6 followed by CH_2Cl_2/hexanes 1:3) afforded **10** (80 mg, 45%). Yellow semisolid. R_f 0.3 (hexane/CH_2Cl_2 2:1). UV/VIS ($CHCl_3$): 292 (20900), 385 (19100). IR (CH_2Cl_2, cast): 3052, 2954, 2924, 2187, 2147, 1608, 1519, 1362. ^{1}H-NMR (300 MHz, $CDCl_3$): 7.52–7.43 (*m*, 4 H); 7.34–7.24 (*m*, 6 H); 7.16 (*d*, *J* = 9.0, 2 H); 6.58 (*d*, *J* = 9.0, 2 H); 2.95 (*s*, 6 H); 0.92 (*t*, *J* = 8.0, 9 H); 0.55 (*q*, *J* = 8.0, 6 H). ^{13}C-NMR (75.5 MHz, $CDCl_3$): 154.4; 150.0; 140.7; 140.5; 132.6; 130.43; 130.39; 128.1; 128.0; 127.51; 127.48; 111.7; 110.2; 104.9; 102.8; 95.0; 93.4; 87.2; 40.2; 7.4; 4.3. HR-EI-MS: 461.2545 ($C_{32}H_{35}NSi^+$, M^+; calc. 461.2539).

1-[4-(Dimethylamino)phenyl]-3-(diphenylethylidene)-1-(4-nitrophenyl)penta-1,4-diyne (=*4-[3-(Diphenylethylidene)-5-(4-nitrophenyl)penta-1,4-diynyl]*-N,N-*dimethylbenzenamine*; **11**). According to the *G. P.*, with **10** (65 mg, 0.14 mmol) and 1M Bu_4NF in THF (0.3 ml) in wet THF (20 ml), then with 1-iodo-4-nitrobenzene (42 mg, 0.17 mmol), deoxygenated Et_3N (20 ml), THF (20 ml), [$PdCl_2(PPh_3)_2$] (6 mg, 0.009 mmol), and CuI (4 mg, 0.02 mmol) for 17 h. CC (silica gel *H*, hexane/CH_2Cl_2 3:1) afforded **11** (50 mg, 76%). Red solid. M.p. 108–110°. R_f 0.56 (hexane/CH_2Cl_2 1:2). UV/VIS ($CHCl_3$): 272 (sh, 21000), 291 (24300), 367 (31300). IR (CH_2Cl_2, cast): 2925, 2185, 1607, 1516, 1340. ^{1}H-NMR (300 MHz, $CDCl_3$): 8.16 (*d*, *J* = 9.0, 2 H); 7.63–7.58 (*m*, 2 H); 7.56–7.50 (*m*, 2 H); 7.48–7.36 (*m*, 8 H); 7.27 (*d*, *J* = 8.8, 2 H); 6.67 (*d*, *J* = 8.8, 2 H); 3.02 (*s*, 6 H). ^{13}C-NMR (75.5 MHz, $CDCl_3$, APT): 156.0; 150.2; 146.8; 140.7; 140.2; 132.8; 132.1; 130.6 (2×); 130.3; 128.7; 128.6; 127.8; 127.7; 123.5; 111.9; 102.0; 94.9; 94.1; 89.4; 86.3; 40.2 (one coincident signal not observed). HR-EI-MS: 468.1833 ($C_{32}H_{24}N_2O_2^+$, M^+; calc. 468.1838).

X-Ray Single-Crystal Structure Analyses. Single crystals of **3b**, **4b**, **7**, and **8** suitable for X-ray-analysis were obtained at −4° from MeOH/CH_2Cl_2. Crystal diffraction data were collected with a *Bruker-SMART-1000-CCD* area detector used in combination with a *P4* diffractometer/rotating-anode generator (**3b** and **4b**) or with a *Platform* diffractometer/sealed-tube generator (**7** and **8**). Structures were solved with the program SHELXS-86 [35] (**3b**, **4b**, and **8**) or the DIRDIF-96 [36] program system (**7**). Refinement was completed with the program SHELXL-93[4]) [37]. CCDC-611083 (**3b**), CCDC-611086 (**4b**), CCDC-611085 (**7**), and CCDC-611084 (**8**) contain the supplementary crystallographic data for this paper. These data can be obtained free of charge *via* http://www.ccdc.cam.ac.uk/data_request/cif from the *Cambridge Crystallographic Data Centre*. Details of the structure determinations are given in *Table 7*.

DOKE Experiments. The molecular second hyperpolarizabilities γ were determined by a differential optical *Kerr* effect (DOKE) experimental setup as reported elsewhere [26]. A multi-pass Ti/sapphire laser amplifier was used, with output wavelength 800 nm, pulse width 90 fs, and a repetition rate of *ca.* 1 kHz. The laser beam was split into pump and probe beams, at a greater than 10:1 power ratio. When

---

[4]) Refinement on F_o^2 for all reflections (all of these having $F_o^2 \geq -3\sigma(F_o^2)$). Weighted *R*-factors wR_2 and all goodnesses of fit *S* are based on F_o^2; conventional *R*-factors R_1 are based on F_o, with F_o set to zero for negative F_o^2. The observed criterion of $F_o^2 > 2\sigma(F_o^2)$ is used only for calculating R_1, and is not relevant to the choice of reflections for refinement. *R*-Factors based on F_o^2 are statistically about twice as large as those based on F_o, and *R*-factors based on all data will be even larger.

Table 7. *Crystallographic Experimental Details*

	4b	**3b**	**7**	**8**
Formula	$C_{25}H_{37}NSi$	$C_{23}H_{31}NO_2Si$	$C_{26}H_{25}FeN$	$C_{24}H_{19}FeNO_2$
M_r	379.65	381.58	407.32	409.25
Crystal size [mm]	$0.42 \times 0.22 \times 0.18$	$0.45 \times 0.22 \times 0.18$	$0.59 \times 0.38 \times 0.09$	$0.40 \times 0.19 \times 0.04$
T [°]	22	−80	−80	−80
Crystal system	triclinic	triclinic	monoclinic	monoclinic
Space group	$P\bar{1}$ (No. 2)	$P\bar{1}$ (No. 2)	$P2_1/c$ (No. 14)	$P2_1$ (No. 4)
a [Å]	8.8003 (6)	7.7041 (5)	19.3515 (17)	12.4819 (9)
b [Å]	13.6654 (10)	11.2582 (8)	10.0900 (9)	6.0734 (5)
c [Å]	20.8790 (14)	13.1958 (9)	10.4497 (9)	12.6720 (10)
α [°]	90.784 (1)	84.7476 (12)		
β [°]	94.888 (1)	82.7816 (16)	90.5693 (18)	94.7813 (14)
γ [°]	93.144 (1)	77.0706 (12)		
V [Å^3]	2497.6 (3)	1104.29 (13)	2040.3 (3)	957.29 (13)
Z	4	2	4	2
$\rho_{calc.}$ [g/cm^3]	1.010	1.148	1.326	1.420
μ [mm^{-1}]	0.103	0.123	0.750	0.807
2θ limit [°]	51.44	52.76	52.82	52.78
Independent reflections	9449	4474	4182	3883
Observed reflections ($F_o^2 \geq 2\sigma(F_o^2)$)	3918	3415	3666	3526
Goodness-of-fit (S) ($F_o^2 \geq -3\sigma(F_o^2)$)	0.840	1.034	1.079	0.997
Final R_1 ($F_o^2 \geq 2\sigma(F_o^2)$)	0.0543	0.0460	0.0321	0.0330
wR_2 [$F_o^2 \geq -3\sigma(F_o^2)$]	0.1477	0.1272	0.0986	0.0769
Largest diff. peak and hole [e Å^{-3}]	0.146, −0.181	0.308, −0.271	0.313, −0.286	0.433, −0.243

the two pulses simultaneously arrive at the sample, the maximum rotation in polarization due to the ultrafast electronic nonlinearity is given by *Eqn. 2* where ϕ and n_2^{I} are complex quantities that can be expressed as $\phi = \phi' + i\phi''$ and $n_2^{\mathrm{I}} = n_2^{\mathrm{I}\prime} + in_2^{\mathrm{I}\prime\prime}$. In theory, these quantities are related to third-order nonlinear optical susceptibility $\chi^{(3)}$ and γ. As established in previous work [26], the relative sample second hyperpolarizability γ_s can be calculated by *Eqn. 3*, where the subscripts S and R correspond to the sample and reference, respectively; L^4 is the *Lorentz* local-field factor, and N_c is the molecular concentration in cm^{-3}. All samples were prepared as solns. in THF and then filtered into 1.0-mm quartz cuvettes through *Nylon* syringe filters for measurement. By altering the polarization of the pump pulse, DOKE detection can be used to measure nonlinear absorption (two-photon-absorption) dynamics. Two-photon-absorption (TPA) cross-sections were obtained by iterative scans of samples of interest and a 3.0 mM standard soln. of MPPBT in DMSO [27]. The ultrafast TPA cross-section of the sample is then calibrated to that of the reference sample ($\sigma^{(2)}{}_{\mathrm{MPPBT}} = 380$ GM; $\lambda = 800$ nm) according to [30]:

$$\phi = \frac{2\pi d}{\lambda} n_2^{\mathrm{I}} I_{\mathrm{pump}} \tag{2}$$

$$\langle \gamma_S \rangle = \frac{\mathrm{Re}\left(\chi_R^{(3)}\right)}{L^4 N_c} \left(\frac{\phi_S'}{\phi_R'} - 1\right) \tag{3}$$

$$\sigma_S^{(2)} = \frac{\phi_S''}{\phi_R''} \frac{N_{c_R}}{N_{c_S}} \sigma_R^{(2)} \tag{4}$$

DFT and NBO Analyses. The full geometry optimizations of **18a**–**e** were performed by using the density-functional-theory (DFT) approach, in which *Becke* three-parameters *Lee-Yang-Parr* (B3LYP) hybrid functional was employed together with the 6-31G* basis set [38]. The calculated geometry parameters are in reasonable agreement with those determined in analogous crystal structures. All optimized structures were confirmed to be pure minima by vibrational analysis calculated at the same level. Delocalization energies were calculated by NBO analysis, in which three sets of antibonding orbitals on the g-DEE skeleton (see *Fig. 6*), namely, out-of-plane π*-orbitals, in-plane π*-orbitals, and in-plane σ*-orbitals, were deleted separately. The energy increase after deletion of each set of antibonding orbitals was thus deemed as the delocalization energy contributed by those orbitals. All the calculations were performed with the Gaussian 03 package [39]. The NBO analysis was done by the program NBO 3.1 [40] as implemented in Gaussian 03.

REFERENCES

[1] P. N. Prasad, D. J. Williams, 'Introduction to Nonlinear Optical Effects in Molecules and Polymers', Wiley, New York, 1991.
[2] U. Gubler, C. Bosshard, *Adv. Polym. Sci.* **2002**, *158*, 123–191.
[3] R. R. Tykwinski, U. Gubler, R. E. Martin, F. Diederich, C. Bosshard, P. Günter, *J. Phys. Chem. B* **1998**, *102*, 4451.
[4] R. E. Martin, F. Diederich, *Angew. Chem., Int. Ed.* **1999**, *38*, 1350.
[5] H. Meier, *Angew. Chem., Int. Ed.* **2005**, *44*, 2482.
[6] H. S. Nalwa, in 'Nonlinear Optics of Organic Molecules and Polymers', Eds. H. S. Nalwa and S. Miyata, CRC Press, Boca Raton, FL, 1997, pp. 611–797.
[7] M. B. Nielsen, F. Diederich, *Chem. Rev.* **2005**, *105*, 1837.
[8] M. Bruschi, M. G. Giuffreda, H. P. Lüthi, *ChemPhysChem* **2005**, *6*, 511.
[9] M. Gholami, R. R. Tykwinski, *Chem. Rev.* **2006**, *106*, 4997; R. R. Tykwinski, Y. Zhao, *Synlett* **2002**, 1939.
[10] Y. Zhao, A. D. Slepkov, C. O. Akoto, R. McDonald, F. A. Hegmann, R. R. Tykwinski, *Chem.–Eur. J.* **2005**, *11*, 321.
[11] Y. Zhao, R. McDonald, R. R. Tykwinski, *J. Org. Chem.* **2002**, *67*, 2805.
[12] B. R. Kaafarani, B. Wex, B. Strehmel, D. C. Neckers, *Photochem. Photobiol. Sci.* **2002**, *1*, 942.
[13] S. C. Ciulei, R. R. Tykwinski, *Org. Lett.* **2000**, *2*, 3607.
[14] B. C. van der Wiel, R. M. Williams, C. A. van Walree, *Org. Biomol. Chem.* **2004**, *2*, 3432.
[15] C. A. van Walree, V. E. M. Kaats-Richters, S. J. Veen, B. Wieczorek, J. H. van der Wiel, B. C. van der Wiel, *Eur. J. Org. Chem.* **2004**, 3046.
[16] P. J. Stang, T. E. Fisk, *Synthesis* **1979**, 438.
[17] Y. Zhao, K. Campbell, R. R. Tykwinski, *J. Org. Chem.* **2002**, *67*, 336.
[18] V. Alain, S. Redoglia, M. Blanchard-Desce, S. Lebus, K. Lukaszuk, R. Wortmann, U. Gubler, C. Bosshard, P. Günter, *Chem. Phys.* **1999**, *245*, 51.
[19] L.-T. Cheng, W. Tam, S. R. Marder, A. E. Stiegman, G. Rikken, C. W. Spangler, *J. Phys. Chem.* **1991**, *95*, 10643.
[20] F. Diederich, *Chem. Commun.* **2001**, 219.
[21] S. Nikas, N. A. Rodios, A. Varvoglis, A. Terzis, C. P. Raptopoulou, *J. Heterocycl. Chem.* **1996**, *33*, 997.
[22] D. A. Shultz, H. Lee, R. K. Kumar, K. P. Gwaltney, *J. Org. Chem.* **1999**, *64*, 9124.
[23] R. R. Tykwinski, M. Schreiber, R. Pérez Carlón, F. Diederich, V. Gramlich, *Helv. Chim. Acta* **1996**, *79*, 2249.
[24] S. Szafert, J. A. Gladysz, *Chem. Rev.* **2003**, *103*, 4175.
[25] C. Bosshard, P. Günter, in 'Nonlinear Optics of Organic Molecules and Polymers', Eds. H. S. Nalwa and S. Miyata, CRC Press, Boca Raton, FL, 1997, Chapt. 6.
[26] A. D. Slepkov, F. A. Hegmann, Y. Zhao, R. R. Tykwinski, K. Kamada, *J. Chem. Phys.* **2002**, *116*, 3834.
[27] K. Kamada, K. Ohta, I. Yoichiro, K. Kondo, *Chem. Phys. Lett.* **2003**, *372*, 386.

[28] A. Hilger, J.-P. Gisselbrecht, R. R. Tykwinski, C. Boudon, M. Schreiber, R. E. Martin, H. P. Lüthi, M. Gross, F. Diederich, *J. Am. Chem. Soc.* **1997**, *119*, 2069.
[29] J. P. Gisselbrecht, N. N. P. Moonen, C. Boudon, M. B. Nielsen, F. Diederich, M. Gross, *Eur. J. Org. Chem.* **2004**, 2959.
[30] Y. Zhao, Y. Shirai, A. D. Slepkov, L. Cheng, L. B. Alemany, T. Sasaki, F. A. Hegmann, J. M. Tour, *Chem.–Eur. J.* **2005**, *11*, 3643.
[31] N. F. Phelan, M. Orchin, *J. Chem. Ed.* **1968**, *45*, 633.
[32] A. E. Reed, R. B. Weinstock, F. Weinhold, *J. Chem. Phys.* **1985**, *83*, 735.
[33] M. Bruschi, M. G. Giuffreda, H. P. Lüthi, *Chem.–Eur. J.* **2002**, *8*, 4216.
[34] S. Eisler, R. McDonald, G. R. Loppnow, R. R. Tykwinski, *J. Am. Chem. Soc.* **2000**, *122*, 6917.
[35] G. M. Sheldrick, SHELXL-93, Program for Crystal Structure Determination. University of Göttingen, Germany, 1993.
[36] P. T. Beurskens, G. Beurskens, W. P. Bosman, R. de Gelder, S. Garcia Granda, R. O. Gould, R. Israel, J. M. M. Smits, The DIRDIF-96 Program System, Crystallography Laboratory, University of Nijmegen, The Netherlands, 1996.
[37] G. M. Sheldrick, *Acta Crystallogr. Sect. A* **1990**, *46*, 467.
[38] P. J. Stephens, F. J. Devlin, C. F. Chabalowski, M. J. Frisch, *J. Phys. Chem.* **1994**, *98*, 11623.
[39] M. J. Frisch, G. W. Trucks, H. B. Schlegel, G. E. Scuseria, M. A. Robb, J. R. Chesseman, J. A. Montgomery Jr., T. Vreven, K. N. Kudin, J. C. Burant, J. M. Millam, S. S. Iyengar, J. Tomasi, V. Barone, B. Mennucci, M. Cossi, G. Scalmani, N. Rega, G. A. Petersson, H. Nakatsuji, M. Hada, M. Ehara, K. Toyota, R. Fukuda, J. Hasegawa, M. Ishida, T. Nakajima, Y. Honda, O. Kitao, H. Nakai, M. Klene, X. Li, J. E. Knox, H. P. Hratchian, J. B. Cross, V. Bakken, C. Adamo, J. Jaramillo, R. Gomperts, R. E. Stratmann, O. Yazyev, A. J. Austin, R. Cammi, C. Pomelli, J. W. Ochterski, P. Y. Ayala, K. Morokuma, G. A. Voth, P. Salvador, J. J. Dannenberg, V. G. Zakrzewski, S. Dapprich, A. D. Daniels, M. C. Strain, O. Farkas, D. K. Malick, A. D. Rabuck, K. Raghavachari, J. B. Foresman, J. V. Ortiz, Q. Cui, A. G. Baboul, S. Clifford, J. Cioslowski, B. B. Stefanov, G. Liu, A. Liashenko, P. Piskorz, I. Komaromi, R. L. Martin, D. J. Fox, T. Keith, M. A. Al-Laham, C. Y. Peng, A. Nanayakkara, M. Challacombe, P. M. W. Gill, B. Johnson, W. Chen, M. W. Wong, C. Gonzalez, J. A. Pople, Gaussian, Inc., Wallingford CT, 2004.
[40] E. D. Glendening, A. E. Reed, J. E. Carpenter, F. Weinhold, NBO Version 3.1, Theoretical Chemistry Institute, University of Wisconsin, Madison, 2001.

Received January 4, 2007